Journal of Solid State Chemistry **160,** 69–76 (2001)
doi:10.1006/jssc.2000.9193, available online at http://www.idealibrary.com on IDEAL®

Synthesis of Layered-Type Hydrous Manganese Oxides from Monoclinic-Type $LiMnO_2$

Ramesh Chitrakar,[1] Hirofumi Kanoh, Yang-Soo Kim, Yoshitaka Miyai, and Kenta Ooi[1]

National Institute of Advanced Industrial Science and Technology 2217-14 Hayashi-cho, Takamatsu 761-0395, Japan

Received January 16, 2001; in revised form March 22, 2001; accepted March 26, 2001; published online May 30, 2001

Layered-type hydrous manganese oxides $MnO_2 \cdot 0.70H_2O$ and $MnO_2 \cdot 0.22H_2O$ with almost the same rod shape morphology as that of the precursor monoclinic-type $LiMnO_2$ were synthesized. The structural transformations from monoclinic-type $LiMnO_2$ to a birnessite-type $MnO_2 \cdot 0.70H_2O$ took place after lithium in $LiMnO_2$ was extracted with 0.1 mol dm^{-3} $(NH_4)_2S_2O_8$ solution without dissolution of manganese. The extraction of lithium from $LiMnO_2$ with 0.5 mol dm^{-3} HCl solution followed by the dissolution of manganese formed a trigonal-type $MnO_2 \cdot 0.22H_2O$. The maximum ion exchange capacity of $MnO_2 \cdot 0.22H_2O$ toward alkali metal ions was found to be only 3 mmol/g; the material did not show any ion sieve properties. The pH titration study suggested that the $MnO_2 \cdot 0.22H_2O$ was a weak acidic adsorbent which was found to be a metastable phase.

Key Words: **lithium manganese oxide; ion exchange; morphology; metastable phase.**

INTRODUCTION

Lithium manganese oxides with spinel and layered structures have been investigated as adsorbents (1–6) or as electrode materials in rechargeable lithium batteries (7–10). Materials such as λ-MnO_2, $H_{1.33}Mn_{1.67}O_4$, and $MnO_2 \cdot 0.5H_2O$ derived from the precursors $LiMn_2O_4$, $Li_{1.33}Mn_{1.67}O_4$, and $Li_{1.6}Mn_{1.6}O_4$, respectively, are known as lithium selective adsorbents. The structural characteristics of $LiMn_2O_4$ and $Li_{1.33}Mn_{1.67}O_4$ and their lithium extraction/insertion reactions have been extensively studied by Ammundsen *et al.* (11–15). Layered structures are of interest as cathodes in lithium rechargeable batteries. However, lithium manganese oxides with layered structure are not thermodynamically stable. Among the layered materials, lithium cobalt oxide and lithium nickel oxide are most stable to lithium intercalation/deintercalation reactions and these materials are extensively used in lithium batteries (16, 17). We are presently interested in the synthesis of new materials based on manganese compounds for use as adsorbents.

Orthorhombic-type $LiMnO_2$, having an ordered rock salt structure of space group *Pmnm*, transformed irreversibly to spinel-type material upon electrochemical cycling (10). Similar structural transformation has been reported after orthorhombic-type $LiMnO_2$ was treated with aqueous ammonium peroxodisulphate solution (18).

Armstrong and Bruce first reported the preparation of pure crystalline monoclinic-type $LiMnO_2$ by an ion exchange reaction from α-$NaMnO_2$ (19). Recently a monoclinic-type $LiMnO_2$ with trace impurities of orthorhombic-type $LiMnO_2$ and Li_2MnO_3 was synthesized directly from Mn_2O_3 by hydrothermal reaction at 220°C using mixed solutions of LiOH and KOH or LiCl and KOH (20). Monoclinic-type $LiMnO_2$ is not thermodynamically stable, because lithium extraction from and reinsertion into $LiMnO_2$ is not a reversible intercalation reaction (19–21). Monoclinic-type $LiMnO_2$ transforms into spinel-related form during electrochemical cycling. The preparation of metal-doped layered $LiMnO_2$ (monoclinic) has received considerable attention due to its possible use as a cathode material, because the metal-doped $LiMnO_2$ does not easily convert to the spinel type upon electrochemical cycling (22, 23). Chromium and aluminum (as little as 5%) are the best dopants in suppressing the transformation of monoclinic-type $LiMnO_2$ to spinel. Substitution of a small fraction (as little as 5%) of Mn with Al or Cr is within the Mn sites in the layered structure.

Recently the structural characterizations of monoclinic-type $LiMnO_2$ were investigated to examine the effect of chemical and electrochemical delithiation/relithiation reactions on electronic configuration and crystal structure (24).

Detailed studies on lithium extraction from monoclinic-type $LiMnO_2$ using HCl solution or $(NH_4)_2S_2O_8$ solution have not been done. The present study is focused on the preparation of layered-type manganese oxides from monoclinic-type $LiMnO_2$ and their alkali metal ion adsorption properties.

[1] To whom correspondence should be addressed. Fax: +81-87-869-3550. E-mail: chitrak@sniri.go.jp; ooi@sniri.go.jp.

0022-4596/01 $35.00

EXPERIMENTAL SECTION

Preparation of $LiMnO_2$

The α-$NaMnO_2$ was obtained by heating a mixture of α-Mn_2O_3 and Na_2CO_3 (Na/Mn = 1) in a closed crucible at 800°C for 24 h in air, quenching to room temperature and grinding, after which the process was repeated once more. The α-$NaMnO_2$ was stored in a desiccator because the material was very hygroscopic in nature. In the hydrothermal method, 2 g of α-$NaMnO_2$ was mixed with 10 g of LiBr in 40 cm^3 *n*-hexanol and autoclaved at 155°C for 6 h in a 50 cm^3 Teflon-lined stainless steel vessel; the obtained product $LiMnO_2$ was washed with *n*-hexanol and then methanol and then air-dried.

Physical Analysis

X-ray diffraction analysis was carried out using a Rigaku type RINT 1200 X-ray diffractometer with a graphite monochromator. DTA-TG curves of the materials were obtained on a MAC Science thermal analyzer (System 001 200 TG-DTA) at a heating rate of 10°C/min. Water contents of the samples were calculated from the weight loss after heating at 400°C. Infrared spectra were obtained by the KBr pellet method using a Perkin Elmer System 2000 infrared spectrophotometer. SEM observations of various samples were carried out on a Hitachi type S-2460 N scanning electron microscope.

Chemical Analysis

The different materials (50 mg) were dissolved in 0.5 mol dm^{-3} of hydrochloric acid solution containing hydrogen peroxide and the lithium, sodium, and manganese contents were determined with Shimadzu AA-760 atomic absorption spectrometer. The mean oxidation number of manganese (Z_{Mn}) was evaluated after determining the available oxygen by standard oxalic acid method (25).

pH Titration

A 0.10-g sample of acid-treated material ($MnO_2 \cdot 0.22H_2O$) was immersed in 10 cm^3 of mixed solution (0.1 mol dm^{-3} $MCl + MOH$, M = alkali metal ions) at various ratios with intermittent shaking at room temperature for 2 weeks. After the attainment of equilibrium, the alkali metal contents in the supernatant solution were determined by atomic absorption spectrometry and the pH of the solution was determined with a Horiba type pH meter, Model M-13.

Extraction of Lithium from $LiMnO_2$

The extraction of lithium from $LiMnO_2$ was determined by stirring 1 g of material with 1 dm^3 of 0.5 mol dm^{-3} HCl solution for 1 day or 0.1 mol dm^{-3} $(NH_4)_2S_2O_8$ solution for 2 days. In batch experiment, 0.10 g of $LiMnO_2$ was treated with 100 cm^3 of 0.5 mol dm^{-3} HCl solution or 0.1 mol dm^{-3} $(NH_4)_2S_2O_8$ solution. Lithium reinsertion into lithium-extracted materials were determined by a batch method using a mixed solution of 0.1 mol dm^{-3} LiOH and LiI.

RESULTS AND DISCUSSION

Characterization of α-$NaMnO_2$ and $LiMnO_2$

The structure of α-$NaMnO_2$ is based on the cubic close-packed network of oxygen in which both the sodium and manganese are located in octahedral sites yielding sandwiches of MnO_2 in the cubic 111 direction, separated by a sodium layer. The crystal structure is a monoclinic distortion (space group $C2/m$) (17, 19). The α-$NaMnO_2$ could be prepared by heating a mixture of manganese oxide (Mn_2O_3) and sodium carbonate at a temperature of 700–800°C in flowing argon, nitrogen, or air (19, 21). We prepared α-$NaMnO_2$ in air and the material was stored in a desiccator. The material was not stable in air, because the brown color was easily transformed to black due to the formation of a more stable phase ($Na_{0.7}MnO_{2.05}$). The chemical formula of $NaMnO_2$ was confirmed from chemical analysis of sodium and manganese and the mean oxidation number of manganese (Z_{Mn}) (Table 1). The XRD pattern of the present material showed that the crystal system was identical to that of α-$NaMnO_2$ (JCPDS No. 25-0845) (Fig. 1). However, the intensity (I_{001}) was higher than the intensities (I_{202} and I_{111}) in the present material, whereas the intensities (I_{202} and I_{111}) were higher than I_{001} in JCPDS No. 25-0845. The XRD pattern of the present material showed traces of $Na_{0.7}MnO_{2.05}$ phase; such trace impurities have been reported by other groups also (21). The lattice parameters of the present material were the same as reported in the literature (21) (Table 2).

TABLE 1
Composition of Different Materials

Material	Na/Mn	Li/Mn	H_2O/Mn	Z_{Mn}	Formula
α-$NaMnO_2$ (monoclinic)	0.99	—	—	3.08	$NaMnO_{2.04}$
$LiMnO_2$ (monoclinic)	0.04	0.96	—	3.05	$Li_{0.97}Na_{0.04}MnO_{2.03}$
$(NH_4)_2S_2O_8$-treated material of $LiMnO_2$ (birnessite)	0.016	0.02	0.70	3.88	$MnO_{1.94} \cdot 0.70H_2O$
HCl-treated material of $LiMnO_2$ (trigonal)	0.03	0.02	0.22	3.96	$MnO_{1.98} \cdot 0.22H_2O$

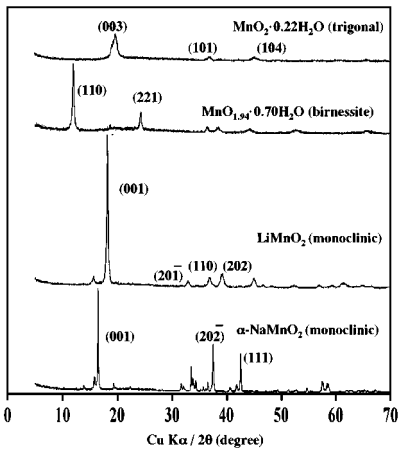

FIG. 1. XRD patterns of different materials.

TABLE 2
Lattice Parameters of Different Materials

Materials	Present work	Literature cited
α-$NaMnO_2$	$a = 5.67$ Å $b = 2.86$ Å $c = 5.81$ Å $\beta = 113.10°$ (Monoclinic)	$a = 5.66$ Å $b = 2.86$ Å $c = 5.80$ Å $\beta = 113.13°$ (Monoclinic) (Ref. 21)
$LiMnO_2$	$a = 5.44$ Å $b = 2.81$ Å $c = 5.41$ Å $\beta = 116.22°$ (Monoclinic)	$a = 5.44$ Å $b = 2.81$ Å $c = 5.39$ Å $\beta = 116.01°$ (Monoclinic) (Ref. 19)
$MnO_2 \cdot 0.70H_2O$	$a = 8.45$ Å $b = 14.89$ Å $c = 17.67$ Å (Birnessite)	$a = 8.52$ Å $b = 14.76$ Å $c = 17.54$ Å (Birnessite) (JCPDS No. 23-1239)
$MnO_2 \cdot 0.22H_2O$	$a = 2.85$ Å $c = 13.59$ Å (Trigonal)	$a = 2.8$ Å $c = 13.4$ Å (Trigonal) (Ref. 27)

The monoclinic-type $LiMnO_2$ was prepared by refluxing α-$NaMnO_2$ in a mixture of LiBr and *n*-hexanol (19, 21). In the present study, we adopted a hydrothermal method; the exchange of sodium with lithium in α-$NaMnO_2$ was completed within 3 h. A complete exchange of sodium ions with lithium ions could not be achieved; only 95% of sodium ions could be exchanged. Such an incomplete exchange reaction was also reported by other groups (19, 21). The formula of $LiMnO_2$ was confirmed from the chemical analysis of lithium and manganese and Z_{Mn} value (Table 1).

The XRD pattern of $LiMnO_2$ is shown in Fig. 1. All the peaks could be indexed to a monoclinic structure with space group $C2/m$. The intensity (I_{001}) was higher than other peak intensities in the present material. The lattice parameter c was slightly greater than that reported in the literature value (19), while other lattice parameters a and b were nearly the same (Table 2). The structure of $LiMnO_2$ is an ordered rock salt structure with edge-sharing MnO_2 octahedra linked to form MnO_2 layers. The MnO_2 sheets are separated by sheets of octahedrally coordinated lithium ions. The sheets of positively charged lithium ions effectively screen and stabilize negatively charged MnO_2 layers (Fig. 2, right).

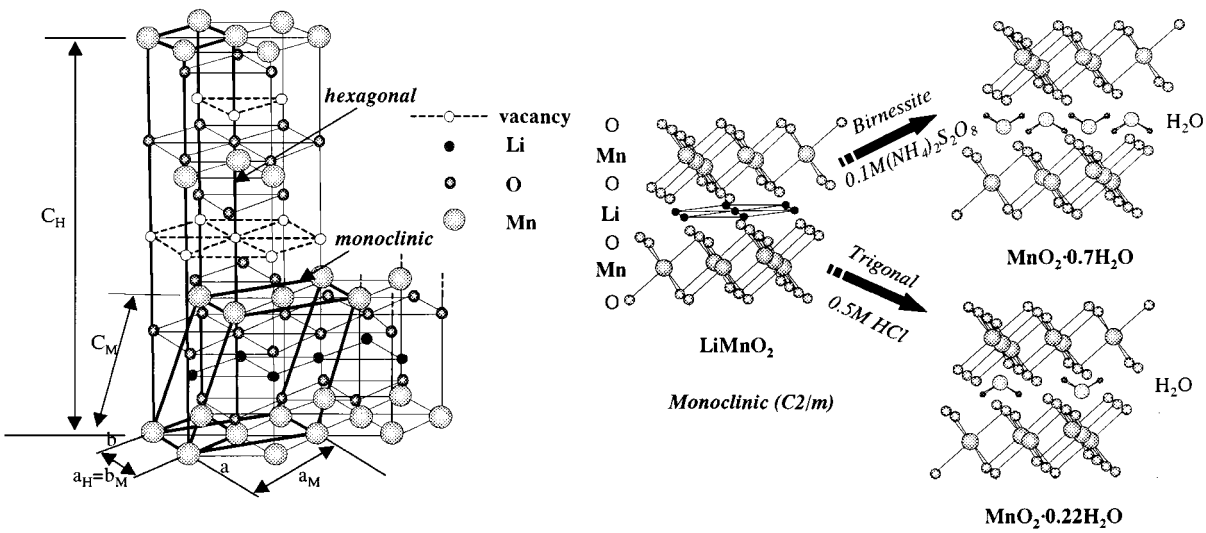

FIG. 2. Schematic representation of structural transformation of monoclinic $LiMnO_2$ to trigonal $MnO_2 \cdot 0.22H_2O$ in hexagonal settings (left) and phase transformations from monoclinic to birnessite and trigonal phases (right).

FIG. 3. SEM images of $LiMnO_2$ (top), $MnO_2 \cdot 0.70H_2O$ (middle), and $MnO_2 \cdot 0.22H_2O$ (bottom).

The structure of $LiMnO_2$ is very close to the structure of α-$NaMnO_2$.

The SEM image of $LiMnO_2$ showed rod-shaped crystals of about 10 μm in length and 1 μm in breadth (Fig. 3, top). This is likely to be an effect of preferred orientation. The rod shape crystallites might be due to effect of preferred orientation. Such large crystals have not been reported in the literature.

IR spectra of $LiMnO_2$ showed only absorption bands at 488 and 648 cm^{-1} which could be assigned to the Mn–O stretching vibrations. The DTA-TG curve of $LiMnO_2$ showed a broad exothermic peak around 450°C with weight gain (Fig. 4, bottom). The weight gain reached its maximum at 600°C and then decreased slightly with a rise in temperature above 600°C. The total weight gain was about 4.6%. We could assume the decomposition of $LiMnO_2$ above 450°C into a mixture of $LiMn_2O_4$ and Li_2MnO_3 because some peaks of Li_2MnO_3 were detected in the XRD pattern and only 70% of lithium was extracted from the heated material with 0.5 mol dm^{-3} HCl solution.

Characterization of $MnO_2 \cdot 0.70\ H_2O$ and $MnO_2 \cdot 0.22H_2O$

The extraction of Li^+ from $LiMnO_2$ was investigated with 0.1 mol dm^{-3} $(NH_4)_2S_2O_8$ solution. The complete extraction of lithium (99%) from $LiMnO_2$ was achieved in 2 days with negligible dissolution of manganese (Fig. 5, bottom). This showed that the extraction proceeded by the redox-type reaction, which can be described similar to that for the orthorhombic-type $LiMnO_2$ (18). The redox-type reaction can be written as follows:

$$2\mathrm{LiMn(III)O_2} + x\mathrm{S_2O_8^{2-}} \rightarrow 2\mathrm{Li_{1-x}Mn(III)_{1-x}Mn(IV)_xO_2} + 2x\mathrm{Li^+} + 2x\mathrm{SO_4^{2-}}.$$

In the present study, the structural transformation of monoclinic-type $LiMnO_2$ to birnessite-type material was

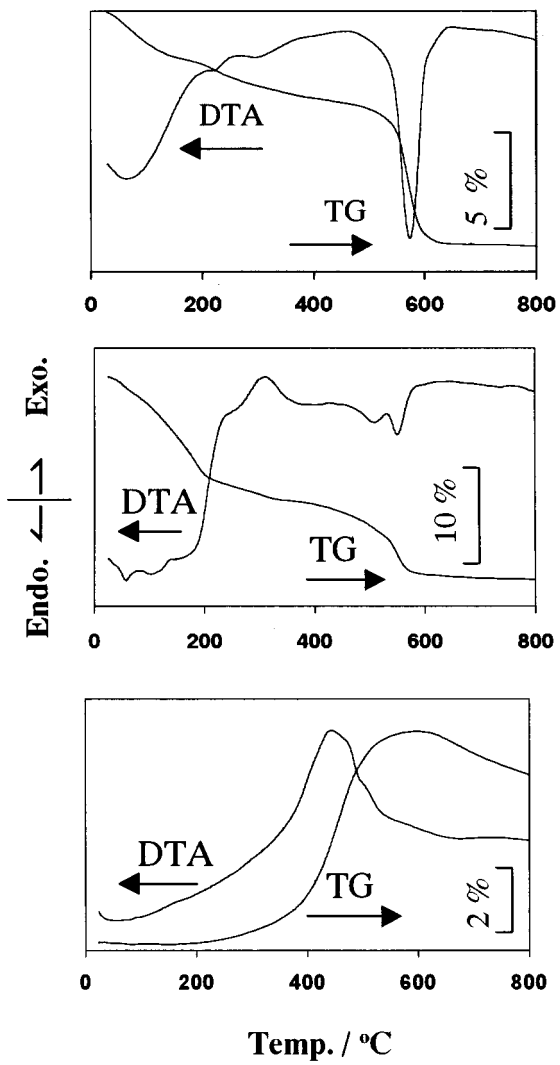

FIG. 4. DTA-TG curves of $LiMnO_2$ (bottom), $MnO_2 \cdot 0.7H_2O$ (middle) and $MnO_2 \cdot 0.22H_2O$ (top).

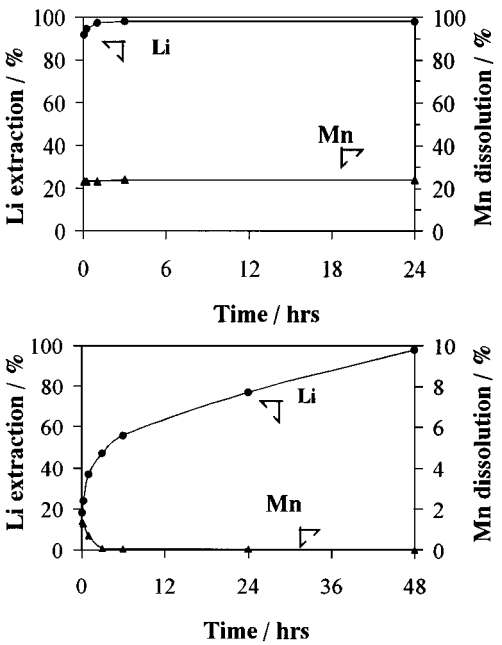

FIG. 5. Extraction of lithium from $LiMnO_2$ with 0.1 mol dm^{-3} $(NH_4)_2S_2O_8$ solution (bottom) and with 0.5 mol dm^{-3} HCl solution (top). $LiMnO_2$, 0.10 g; vol, 100 cm^3; temp, room temp.

observed. A schematic representation of the phase transformation is shown in Fig. 2 (right). The structure of $LiMnO_2$ having flat edge-shared MnO_6 octahedral layers is similar to the birnessite phase with water molecules between the MnO_6 octahedral layers. Since $LiMnO_2$ precursor has a layered structure, it is reasonable to think that layered manganese forms after lithium is extracted by the redox mechanism. The interlayer distance was increased from 4.8 Å in $LiMnO_2$ to 7.3 Å in the birnessite phase. Under similar conditions, a different structural transformation of the orthorhombic-type $LiMnO_2$ with a rock salt structure to a spinel like material was reported (18). The chemical analysis of $LiMnO_2$ after treating with $(NH_4)_2S_2O_8$ solution is given in Table 1. The mean oxidation of manganese was about 3.9. The water content was determined from the weight loss after heating the material at 400°C.

The XRD patterns showed a birnessite-type phase (Fig. 1). The peak intensity of the (001) plane of $LiMnO_2$ decreased after 15 min; the peak almost disappeared after 6 h of lithium extraction. The new peak of the (110) plane of the birnessite-type phase appeared and the intensity of the peak increased as the lithium extraction proceeded overtime. All the peaks could be indexed to the orthorhombic system with birnessite-type structure. The SEM image of the birnessite-type phase retained almost the same morphology as the precursor $LiMnO_2$ (Fig. 3, middle). IR spectra of $MnO_2 \cdot 0.70H_2O$ showed two absorption bands around 3523 and 3146 cm^{-1} which could be assigned to the stretching vibration of hydroxyl groups. The absorption bands between 400 and 700 cm^{-1} due to Mn–O vibrations changed slightly after lithium was extracted from $LiMnO_2$. The DTA-TG curve of the birnessite-type phase showed two endothermic peaks around 60 and 100°C with weight loss, which could be attributed to the dehydration of OH groups (Fig. 4, middle). A small endothermic peak around 550°C could be assigned to the formation of α-Mn_2O_3.

Lithium reinsertion into $MnO_2 \cdot 0.70H_2O$ was determined using a mixed solution of 0.1 mol dm^{-3} of LiOH and LiI. Only 3.5 mmol/g of lithium could be reinserted; the XRD pattern was the same as the original $MnO_2 \cdot 0.70H_2O$. This study showed that lithium extraction from $LiMnO_2$ by $(NH_4)_2S_2O_8$ solution was an irreversible reaction.

Lithium ions were extracted from $LiMnO_2$ with 0.5 mol dm^{-3} HCl solution, the time required for the extraction was very short (Fig. 5, top). The layered structure of $LiMnO_2$ becomes unstable upon extraction of interlayer lithium ions and water molecules enter the interlayer space. The mechanism involved in chemical extraction of lithium from $LiMn_2O_4$ was first reported by Hunter (2). A redox mechanism was proposed for the extraction of lithium from $LiMn_2O_4$ with H_2SO_4, involving the disproportionation of lattice Mn(III) to give a dissolved Mn(II) and a Mn(IV) oxide phase, called λ-MnO_2, which does not contain water molecules. In our present case, a similar mechanism seems to be supported by the experimental data, which showed 25% dissolution of manganese during lithium extraction from $LiMnO_2$ with HCl solution. The Li/Mn mole ratio in the supernatant solution after acid treatment was about 2.05, which was very close to the theoretical value (Li/Mn = 2.0) based on the disproportionation reaction as shown below:

$$3\mathrm{LiMn(III)O_2} + 4x\mathrm{H^+} \rightarrow \mathrm{Li_{3-2x}Mn(III)_{3-2x}Mn(IV)_x}$$

$$\mathrm{O_{6-2x}} + x\mathrm{Mn^{2+}} + 2x\mathrm{Li^+} + 2x\mathrm{H_2O}.$$

The chemical analysis of acid treated material is given in Table 1. The oxidation state of manganese was 4 with a low H_2O/Mn ratio and with a negligible Li/Mn mole ratio.

The acid treated $LiMnO_2$ material showed a simple weak XRD pattern as compared to the original $LiMnO_2$ (Fig. 1). Following the acid treatment, the (001) plane, relating to the interlayer distance between MnO_2 layers of $LiMnO_2$, was shifted to the (003) plane, relating to the interlayer distance between MnO_2 layers of a new phase at a higher angle, indicating the lattice contraction caused by lithium deintercalation. The interlayer distance was decreased from 4.8 to 4.5 Å. This XRD pattern of the acid-treated material was almost the same as reported for $LiMnO_2$ treated with H_2SO_4 or electrochemically charged $LiMnO_2$ (24, 26, 27). The transformation from monoclinic to trigonal phase can be achieved only by the migration of manganese ions into

the lithium layer as proposed from TEM (27) and XAS (24) studies. The increase in crystal symmetry occurs because the Mn^{3+} ions are oxidized on delithiation, thereby reducing the Jahn–Teller distortion.

The XRD patterns of acid treated material can be indexed on hexagonal settings with trigonal structure having $R\bar{3}m$ space group (Table 2). Complete lithium removal from monoclinic-type $LiMnO_2$ resulted in the destruction of the core structure. The crystal phase of the solid changed from monoclinic type to a trigonal type with layered structure. Adjacent MnO_2 layers in the acid-treated material exhibit an increase in electrostatic repulsion as negatively charged oxygen–oxygen interactions increase with the removal of positively charged lithium ions. The water molecules resided between the MnO_2 layers to stabilize the layered structure. We depict the structural relationship between monoclinic and hexagonal settings for $LiMnO_2$ and $MnO_2 \cdot 0.22\ H_2O$, respectively, in a similar to that for $LiCoO_2$ material (28) (Fig. 2, left).

The SEM image of $MnO_2 \cdot 0.22H_2O$ showed that the size and shape of the acid-treated material was almost the same as that of the original $LiMnO_2$ (Fig. 3, bottom). The lithium extraction proceeded without change in the particle shape and size of the original rod-shaped material. The layered-type manganese oxide with rod-shaped morphology has not previously been reported in the literature.

IR spectra of the acid treated material showed a small absorption band around 3500 cm^{-1} indicating the presence of hydroxyl groups. The absorption bands around 400 to 700 cm^{-1} due to Mn–O vibrations in the acid treated material were shifted as compared to the original $LiMnO_2$. These shifts have been reported in other acid-treated lithium manganese oxides (4, 6).

The DTA-TG curve of the acid-treated material showed a small endothermic peak around 70°C with weight loss due to the evaporation of hydroxyl groups (Fig. 4, top). The large endothermic peak around 568°C was due the formation of more the stable Mn_2O_3 phase with loss of oxygen.

The pH titration curves of the $MnO_2 \cdot 0.22H_2O$ sample toward alkali metal ions were obtained in a 0.1 ionic strength solution of metal chlorides and metal hydroxides. The titration curves resembled one another and the adsorbent showed a simple monobasic character with low exchange capacity for alkali metal ions, indicating a weak acidic adsorbent (Fig. 6, top). The affinity order was $Cs^+ < K^+ < Rb^+ \simeq Na^+ \simeq < Li^+$ at pH 12, indicating that the present sample had no ion-sieve properties. The ion exchange capacity reached 3.0 mmol/g for Li^+, Na^+, and Rb^+. The experimentally determined exchange capacity is smaller than the theoretical capacity (4.8 mmol/g) based on the chemical formula of $MnO_2 \cdot 0.22H_2O$. An exchange capacity lower than the theoretical capacity has also been observed for conventional manganese oxide (4–6). The number of replaceable protons responsible for the adsorption

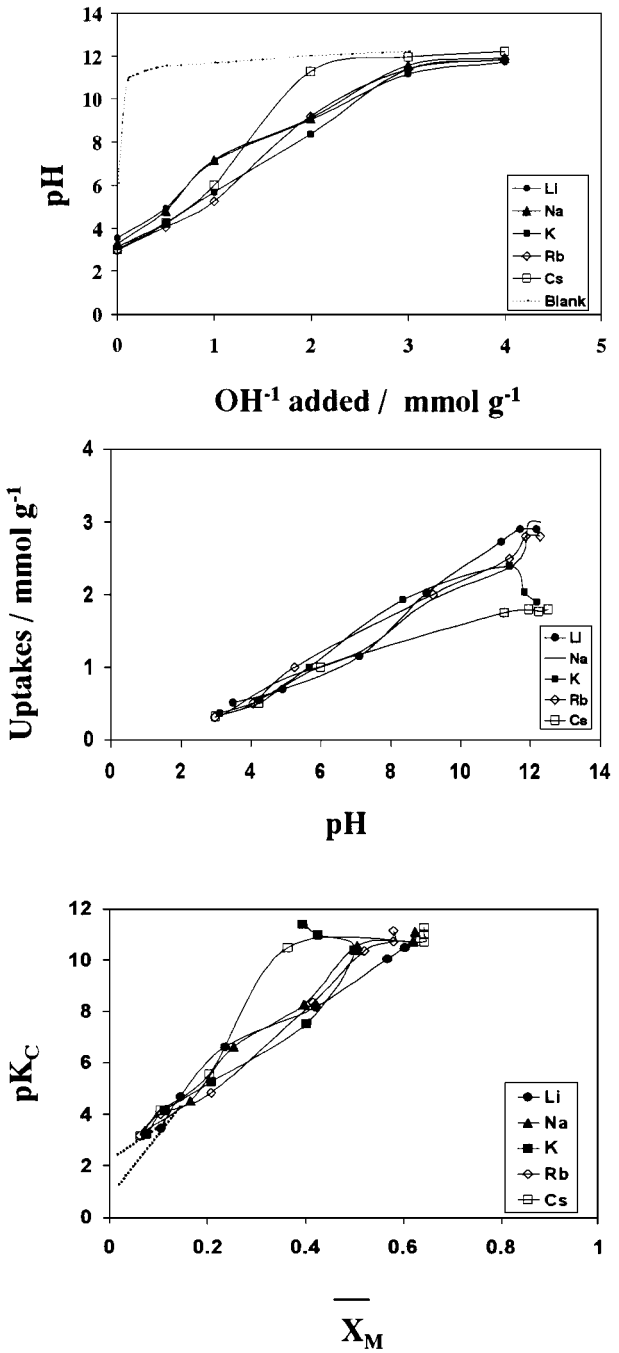

FIG. 6. pH titration curves of $MnO_2 \cdot 0.22H_2O$ toward alkali metal ions (top), pH-dependence of uptake of alkali metal ions (middle), and pK_c vs $\bar{X}_M$ of alkali metal ions (bottom). Adsorbent, 0.10 g; conc., 0.1 mol dm^{-3} (MCL + MOH); vol, 10.0 cm^3; time, 2 weeks.

reactions can be estimated using the difference between a blank run and each titration curve. The apparent capacity (metal ion uptake) thus determined agreed well with the metal ion uptakes determined from the decrease of the metal ion concentration in the supernatant solution (Fig. 6, middle). The uptake of potassium ions decreased above pH

11.5, because the original trigonal phase was transformed into a birnessite phase.

The titration data can be analyzed on the basis of the ion exchange mechanism as follows:

$$\overline{H^+} + M^+ \rightleftarrows \overline{M^+} + H^+, \quad [1]$$

where the bars refer to the species in solid phase. The selectivity coefficient, K, of the above reaction can be defined as

$$K = [a_H + (f_M \overline{X}_M)]/[a_M + (f_H \overline{X}_H)] \quad [2]$$

$$pK_C = -\log K_C = -\log [(a_H \bar{X}_M)/(a_M \overline{X}_H)] \quad [3]$$

$$= pH - \log [\bar{X}_M/(1 - \bar{X}_M)] + \log a_M$$

$$\simeq pH - \log [\bar{X}_M/(1 - \bar{X}_M)] + \log C_M, \quad [4]$$

where $\bar{X}_M$ and $\bar{X}_H$ are the equivalent fractions of M^+ and H^+ in the solid phase, respectively, f_M and f_H are the activity coefficients of the M^+ and H^+ in the solid phase, respectively, and $(a_M +)$ and $(a_H +)$ are the activities of lithium and hydrogen ions in solution, respectively. The K value and standard free energy change (ΔG°) can be evaluated by using a simplified form of Gaines–Thomas equation as follows (28):

$$pK = -\log K = \int_0^1 pK_c \overline{dX_M} \quad [5]$$

$$\Delta G^\circ = (2.303\ RT)\ pK \quad [6]$$

The pK_c values calculated from Eq. [4] above for $MnO_2 \cdot 0.22H_2O$ were plotted against $\overline{X}_M$ in (MCl + MOH) system (Fig. 6, bottom). The pK and ΔG° values calculated are given in Table 3. The intrinsic selectivity coefficients, pK_0, were evaluated by extrapolating the lines in the pK_c vs $\overline{X}_M$ plot to "zero loading" ($\overline{X}_M = 0$) of alkali metal ions. The zero-loading values correspond to the thermodynamic quantities of the hypothetical reaction, where 1 mol of proton is exchanged with 1 mol of alkali metal ions in an infinitesimally dilute fraction of $\bar{X}_M$. From pK_0 values, we can estimate whether the adsorbent shows a strong or weak acidic nature. The pK_0 value of the lithium/proton exchange was found to be 1, whereas for all other metal ions/proton exchanges, similar values of around 2 were observed. The value of pK_0 on zero loading of the ion exchange reaction is a reflection of the action between the adsorption site and ion. These pK_0 values of 1 and 2 indicate that the intrinsic acidity of the exchange sites is stronger than the acidity of (about 4) of typical acid carboxylate.

TABLE 3
Values of pK and ΔG° for $MnO_2 \cdot 0.22H_2O$

System	Concentration (mol dm^{-3})	Temp. (°C)	pK	ΔG° (kJ mol^{-1})
LiCl + LiOH	0.1	25	8.24	47
NaCl + NaOH	0.1	25	8.62	49
KCl + KOH	0.1	25	8.70	50
RbCl + RbOH	0.1	25	8.31	48
CsCl + CsOH	0.1	25	9.33	53

The adsorbent showed a steric hindrance for large ions such as cesium. The free energy changes were positive for all systems, indicating that alkali metal ions are exchanged less preferably on the exchange sites of the adsorbent.

Lithium reinsertion into $MnO_2 \cdot 0.22H_2O$ was determined using a mixed solution of 0.1 mol dm^{-3} of LiOH and LiI. Only 2.5 mmol/g of lithium could be reinserted and the XRD pattern was the same as the original $MnO_2 \cdot 0.22H_2O$. This study showed that lithium extraction from $LiMnO_2$ by HCl solution was an irreversible reaction.

CONCLUSION

A birnessite-type $MnO_2 \cdot 0.70H_2O$ was obtained after $LiMnO_2$ was treated with 0.1 mol dm^{-3} $(NH_4)_2S_2O_8$ solution. A metastable layered structure (trigonal) $MnO_2 \cdot 0.22H_2O$ was obtained after monoclinic-type $LiMnO_2$ was treated with 0.5 mol dm^{-3} HCl solution. The $MnO_2 \cdot 0.22H_2O$ showed no ion-sieve properties. The affinity series for alkali metal ions was $Cs^+ < K^+ < Rb^+ \approx Na^+ \approx Li^+$ at pH 12 and high pK values for alkali metal ions, indicating a weak acidic adsorbent. The high positive values for free energy change indicated that the $MnO_2 \cdot 0.22H_2O$ did not permit the complete exchange reaction of alkali metal ions. Delithiation results in irreversible trivalent manganese oxidation to tetravalent manganese. This in turn reduces the charge on the layers and therefore the capacity to bind ions. The SEM images of $LiMnO_2$, $MnO_2 \cdot 0.22H_2O$ and $MnO_2 \cdot 0.7H_2O$ were almost the same, irrespective of their structures and peak intensities in XRD patterns. Monoclinic-type $LiMnO_2$ was transformed to a mixture of $LiMn_2O_4$ and Li_2MnO_3 after heating at 450°C.

REFERENCES

1. V. V. Vol'khim, G. V. Leont'eva, and S. A. Onorin, *Neorg. Mater.* **9,** 1041 (1973).
2. J. C. Hunter, *J. Solid State Chem.* **39,** 142 (1981).
3. K. Ooi, Y. Miyai, and S. Katoh, *Solvent Extr. Ion Exch.* **5,** 561 (1987).
4. Q. Feng, Y. Miyai, H. Kanoh, and K. Ooi, *Langmuir* **8,** 1861 (1992).
5. Q. Feng, H. Kanoh, and K. Ooi, *J. Mater. Chem.* **9,** 319 (1999).

6. R. Chitrakar, H. Kanoh, Y. Miyai, and K. Ooi, *Chem. Mater*. **12,** 3151 (2000).
7. J. M. Paulsen and J. R. Dahn, *Chem. Mater*. **11,** 3065(1999).
8. J. M. Tarascon and D. Guyomard, *J. Electrochem. Soc*. **138,** 2864 (1991).
9. R. J. Gummow and M. M. Thackeray, *J. Electrochem. Soc*. **141,** 1178 (1994).
10. J. N. Reimers, E. W. Fuller, E. Rossen, and J. R. Dahn, *J. Electrochem. Soc*. **140,** 3396 (1993).
11. B. Ammundsen, G. R. Burns, M. S. Islam, H. Kanoh, and J. Roziere, *J. Phys. Chem. B* **103,** 5175 (1999).
12. B. Ammundsen, J. Roziere, and M. S. Islam, *J. Phys. Chem. B* **101,** 8156 (1997).
13. B. Ammundsen, D. J. Jones, J. Roziere, and G. R. Burns, *Chem. Mater*. **7,** 2151 (1995).
14. B. Ammundsen, D. J. Jones, and J. Roziere, *Chem. Mater*. **10,** 1680 (1998).
15. B. Ammundsen, D. J. Jones, J. Roziere, and G. R. Burns, *Chem. Mater*. **8,** 2799 (1996).
16. T. Ohzuku, A. Ueda, and M. Nagayama, *J. Electrochem. Soc*. **140,** 182 (1993).
17. A. Rougier, P. Gravereau, and C. Delmas, *J. Electrochem. Soc*. **143,** 1168 (1996).
18. W. Tang, H. Kanoh, and K. Ooi, *J. Solid State Chem*. **142,** 19 (1999).
19. A. R. Armstrong and P. G. Bruce, *Nature* **381,** 499 (1996).
20. M. Tabuchi, K. Ado, H. Kobayashi, and H. Kageyama, *J. Electrochem. Soc*. **145,** L49 (1998).
21. G. Vitins and K. West, *J. Electrochem. Soc*. **144,** 2587 (1997).
22. Y.-M. Chiang, D. R. Sadoway, Y.-I. Jang, B. Huang, and H. Wang, *Electrochem. Solid-State Lett*. **2,** 107 (1999).
23. Y.-I. Jang, B. Huang, Y.-M. Chiang, and D. R. Sadoway, *Electrochem. Solid-State Lett*. **1,** 13 (1998).
24. S.-J. Hwang, H.-S. Park, J.-H. Choy, and G. Campet, *Chem. Mater*. **12,** 1818 (2000).
25. Japan Industrial Standard (JIS), M8233 (1969).
26. P. G. Bruce, A. R. Armstrong, and R. L. Gitzendanner, *J. Mater. Chem*. **9,** 193 (1999).
27. Y. Shao-Horn, S. A. Hackney, A. R. Armstrong, P. G. Bruce, R. L. Gitzendanner, C. S. Johnson, and M. M. Thackeray, *J. Electrochem. Soc*. **146,** 2404 (1999).
28. G. L. Gaines and H. C. Thomas, *J. Chem. Phys*. **41,** 714 (1959).